nature structural & molecular biology

Molecular driving forces determining potassium channel slow inactivation

Julio F Cordero-Morales[1–3], Vishwanath Jogini[2,3], Anthony Lewis[2], Valeria Vásquez[1,2], D Marien Cortes[2], Benoît Roux[2] & Eduardo Perozo[2]

K^+ channels undergo a time-dependent slow inactivation process that plays a key role in modulating cellular excitability. Here we show that in the prokaryotic proton-gated K^+ channel KcsA, the number and strength of hydrogen bonds between residues in the selectivity filter and its adjacent pore helix determine the rate and extent of C-type inactivation. Upon channel activation, the interaction between residues at positions Glu71 and Asp80 promotes filter constriction parallel to the permeation pathway, which affects K^+-binding sites and presumably abrogates ion conduction. Coupling between these two positions results in a quantitative correlation between their interaction strength and the stability of the inactivated state. Engineering of these interactions in the eukaryotic voltage-dependent K^+ channel Kv1.2 suggests that a similar mechanistic principle applies to other K^+ channels. These observations provide a plausible physical framework for understanding C-type inactivation in K^+ channels.

In K^+ channels, C-type inactivation is an effective mechanism for controlling the duration of the conductive state through structural rearrangements along the permeation pathway[1,2]. This inactivation process has been linked to conformational changes around the selectivity filter and the extracellular regions of the channel[3–5]. It is inhibited by high extracellular K^+ and the blocker tetraethylammonium (TEA)[6,7], and it can be modulated by permeant ions such as Rb^+ that have a long residence time in the selectivity filter[8] and thus decrease the rate of inactivation[6]. However, the molecular mechanism and conformational changes associated with C-type inactivation remain unresolved, mostly owing to a lack of structural information and a limited understanding of the molecular forces that drive the selectivity filter to adopt its inactivated conformation.

Several pieces of evidence support the idea that a network of interactions behind the selectivity filter has crucial effects on the gating of a number of K^+ channels[9,10]. A point mutation in Kv2.1 (D378E), at a position equivalent to Asp80 in KcsA, affects single-channel behavior by destabilizing the open state[11]. Moreover, mutations in the selectivity filter and pore helix of Shaker, HERG and inward rectifiers also have large effects on gating properties[12–15]. In addition, recent data point to mechanistic equivalence between inactivation in a prokaryotic channel, KcsA (from *Streptomyces lividans*), and C-type inactivation in eukaryotic voltage-dependent K^+ channels[16,17]. In KcsA, the selectivity filter is stabilized by a hydrogen bond network that includes interactions between the carboxylate groups of Glu71 and Asp80 (**Fig. 1a**), between Trp67 and Asp80, and between a buried water bound to the backbone amide nitrogen of Gly79 and Leu81 (ref. 18). Disrupting at least one of these interactions greatly affects the inactivation process in KcsA[17,19]. The Glu71-Asp80 carboxyl-carboxylate interaction is present in other bacterial channels; however, its role there is less well understood[20]. Similar electrostatic interactions also exist in eukaryotic inward rectifiers[21], but they are not typically found in eukaryotic voltage-gated K^+ channels.

We have suggested that the conductive conformation of the selectivity filter is intrinsically unstable owing to interactions between residues in the external vestibule and pore helix[17]. In this model, the movement of TM2 (the inner helix bundle) during gating allows the selectivity filter to fluctuate between conductive and nonconductive conformations before collapsing into the more stable inactivated state. Thus, to understand the molecular basis of C-type inactivation, we needed to identify and characterize the driving forces responsible for the transition between the conductive and deeply inactivated conformations of the K^+ channel selectivity filter. Here, we address two fundamental questions regarding C-type inactivation: the nature of the microscopic forces that drive the transitions from the conductive to the nonconductive state of the selectivity filter, and the putative structural rearrangements leading to inactivation. To this end, we have systematically analyzed the role of the interaction between positions Glu71 and Asp80 in KcsA using functional, spectroscopic, structural and computational approaches, and extended our findings to Kv1.2, a voltage-gated K^+ channel from rat brain.

RESULTS

Functional role of the position 71–Asp80 interaction

To understand the nature of the interaction between Glu71 and Asp80, and its role in C-type inactivation, we systematically analyzed the

[1]Department of Molecular Physiology and Biological Physics, University of Virginia, 1300 JPA, Charlottesville, Virginia 22908, USA. [2]Institute for Molecular Pediatric Sciences, Institute for Biophysical Dynamics and Department of Biochemistry and Molecular Biology, The University of Chicago, 929 E. 57th Street, Chicago, Illinois 60637, USA. [3]These authors contributed equally to this work. Correspondence should be addressed to E.P. (eperozo@uchicago.edu).

Received 22 June; accepted 4 September; published online 7 October 2007; doi:10.1038/nsmb1309

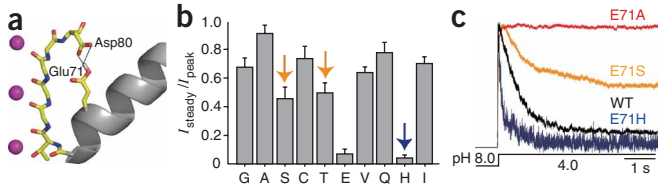

Figure 1 The Glu71-Asp80 interaction is the driving force for inactivation in KcsA. (**a**) A single subunit's P-loop is shown, with a hydrogen bond between the carboxyl group of protonated Glu71 and that of Asp80. (**b**) Ratio of the current at the end of the pH pulse to the peak current (I_{steady}/I_{peak}), from macroscopic current traces, is shown for WT channel and mutants with the residues indicated along the *x*-axis substituted for Glu71. Data shown are means ± s.d. $n > 10$. (**c**) Normalized macroscopic currents activated by pH jump.

functional effects of a series of side chain substitutions at position 71 in the KcsA pore helix (**Fig. 1b**). Of the 15 single point mutations introduced, nine (to glycine, alanine, serine, cysteine, threonine, valine, glutamine, histidine and isoleucine) produced variant channels suitable for electrophysiological analysis. Mutations to tryptophan and proline were not used in this study, to avoid the potential impact of these residues on folding and assembly. Arginine and lysine substitutions severely compromised channel folding and expression. **Figure 1b** shows that most of the mutations yielded functional channels that show low levels of inactivation (glycine, cysteine, valine, glutamine and isoleucine) or only partial inactivation (serine and threonine), where inactivation is quantified as the ratio between the steady-state current and the macroscopic peak current. However, substitution by histidine enhanced not only the rate but also the extent of inactivation after pH-mediated activation (**Fig. 1b**,**c**), presumably by establishing a stronger ionic interaction with Asp80.

Macroscopic current behavior was fully recapitulated at the single-channel level (**Fig. 2a**). At steady state, single-channel recordings of E71H and wild-type (WT) channels are dominated by very long silent periods ($\tau > 10$ s) interrupted by bursts of activity. E71S channels have shorter nonconductive periods ($\tau \sim 1$–2 s), whereas the E71A mutant is characterized by long open times with brief sojourns in nonconductive conformations. As expected, we also found an inverse relationship between the rates of inactivation and the open dwell times of different mutants (**Fig. 2b**). Channels with mutations that remove inactivation (E71A) show long mean open times (~100 ms), whereas the deeply inactivated E71H mutant opens in very brief spikes (mean open times of <2 ms). In addition, the slowest closed-time constant (**Fig. 2b**, red arrow) is directly proportional to the rate of inactivation. These results suggest that the functional effect of each mutation is a consequence of the chemical properties of the mutant's side chain at position 71 and that these properties strongly influence the stability of the conductive conformation of KcsA.

To evaluate the contribution of the selectivity filter and the inner helix bundle gate to the steady-state gating of these mutants, we monitored the conformation of TM2 by EPR spectroscopy (**Fig. 2c**). We generated mutants E71H and E71S in a KcsA background containing the mutation G116C. This cysteine provides a spin-labeling site that reports pH-dependent conformational changes in TM2 (refs. 17,22,23). Comparison of the lineshapes of continuous-wave (CW)-EPR spectra of spin-labeled G116C, E71A G116C, E71S G116C, and E71H G116C mutants at pH 7.0 and 4.0 revealed that the magnitudes of the opening at the lower gate (estimated from the dipolar spectral amplitude ratio) were essentially identical. Thus, the large differences in steady-state nominal open probability (NPo) among these mutants are not due to changes in the behavior of the inner bundle gate, but rather are determined solely by the conformational changes at the selectivity filter.

As a histidine residue could provide a positive charge at position 71, we expected the mutation E71H to restore the interaction between position 71 and 80 that is necessary for inactivation of the selectivity filter[17]. To test the interaction between the imidazolium and carboxylate moieties (His71-Asp80), we analyzed the voltage modulation of KcsA gating (**Fig. 3**)[19]. pH-jump experiments showed that, in contrast to WT KcsA, the rate and extent of inactivation in E71H are enhanced at depolarizing potentials and decreased at hyperpolarizing potentials (**Fig. 3a**,**b**). This inversion in the voltage dependence of inactivation is expected if the transmembrane voltage field promotes a reorientation of the positive imidazolium group, so that at inside positive potentials, the imidazolium group moves toward the Asp80 carboxylate, strengthening the His71-Asp80 interaction (**Fig. 3c**). The opposite voltage

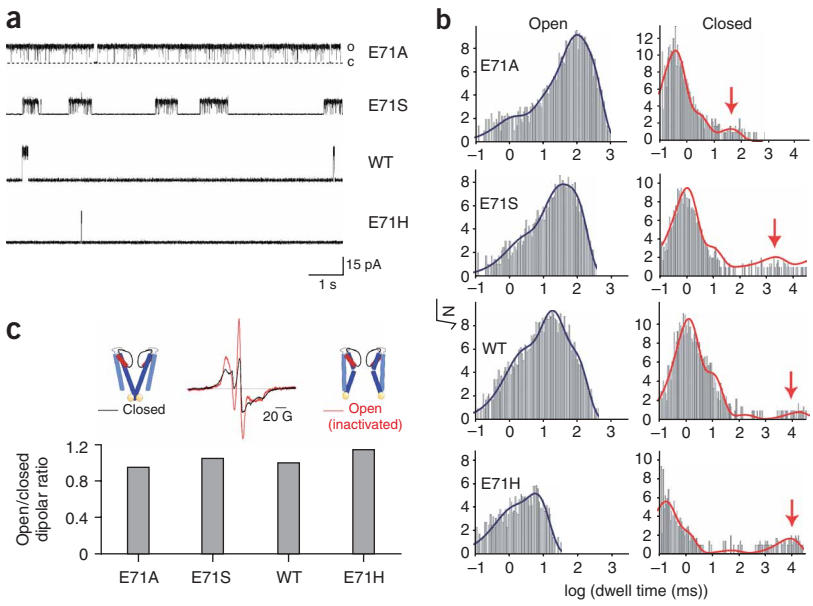

Figure 2 Inverse relationship between the rate of inactivation and the open dwell times. (**a**) Representative single-channel traces from WT channels and Glu71 mutants obtained at pH 4 and +150 mV in symmetric 200 mM KCl solutions. The long closed-time periods characteristic of WT KcsA inactivation (absent in the E71A mutant) are present in single-channel recordings of E71H and, to lesser extent, E71S. (**b**) Dwell-time distribution from recordings in **a**. Red arrow points to the dominant slowest closed-time constant. (**c**) Opening of the intracellular gate, monitored by CW-EPR from spin labels attached at residue G116C (G116C-SL) in a WT background or in the presence of mutations that abolish (E71A G116C-SL) or promote (E71S G116C-SL or E71H G116C-SL) inactivation. Top middle image, representative CW-EPR spectra of spin-labeled G116C obtained from reconstituted channels at pH 7 (black) or pH 4 (red). Bottom, the extent of intracellular gate opening, derived from the amplitude ratio of spectra (dipolar ratio Ω).

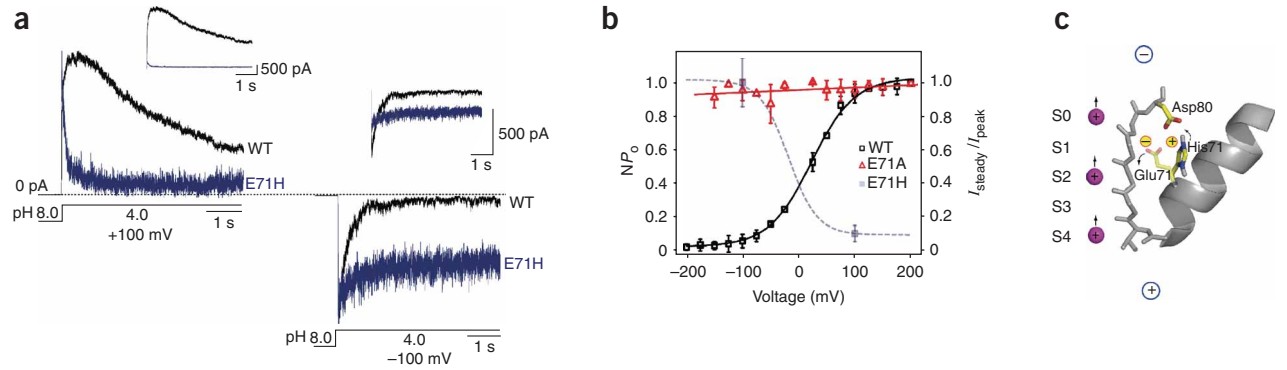

Figure 3 Histidine at position 71 inverts the voltage dependence of inactivation. (**a**) Normalized currents in the E71H mutant show a faster time constant of inactivation at a depolarizing potential (+100 mV, 97 ± 29 ms) and a slower constant at a hyperpolarizing potential (–100 mV, 1212 ± 469 ms) compared to currents in WT channels (+100 mV, 1733 ± 550; –100 mV, 354 ± 59 ms). At potentials where the Glu71 or His71 side chain is oriented towards Asp80, E71H shows a faster time constant of inactivation, suggesting a strong interaction between the pore helix and the external vestibule. Inset shows a comparison of the absolute macroscopic currents between the E71H and WT channels. (**b**) Steady-state NPo-versus-voltage curve from WT channels was fit to a Boltzmann function with a half-point activation ($V_{1/2}$) of 22 mV and a slope parameter (zδ) of 0.72. That from E71A was fit to a linear regression with slope of >0.001. A pseudo Boltzmann curve fit to the two measurements of the E71H macroscopic current (plotted on right *y*-axis) shows the inversion of the voltage dependence; only two data points are included because of the very low channel activity of E71H. Data shown are means ± s.d. $n > 10$. (**c**) Model of voltage-dependent modulation at the KcsA filter.

should accordingly weaken the interaction, as we confirmed experimentally. The inset in **Figure 3a** compares the absolute macroscopic currents of reconstituted E71H and WT channels. Ion current density for the E71H mutant was much lower than for the WT channel, even though the quantity of reconstituted protein was four times larger. Additionally, when WT and E71H channels (each with G116C background mutation) were reconstituted at equal protein/lipid ratios, their EPR spectra showed similar amplitudes, suggesting that there is no difference in the amount of reconstituted channels (**Supplementary Fig. 1** online). These results imply that a large majority of E71H channels either are already pre-inactivated[24,25] or inactivate faster during the activation process[26].

Structural analysis of KcsA inactivation mutants

Because of their differing open probabilities, mutants E71S and E71H represent ideal candidates for the structural investigation of the molecular interactions responsible for C-type inactivation. An initial puzzle was the mechanism by which the E71S mutation influences the open probability (P_o) in KcsA. The serine side chain is not long enough to establish a direct interaction with the Asp80 carboxylate, and thus this mutant should behave like E71A (similar reasoning holds for E71T). A preliminary molecular dynamics simulation of E71S suggested that a water molecule might bridge the interaction between this side chain and Asp80. To test this hypothesis, the crystal structures of the E71S (with tetrabutylammonium, TBA, **Fig. 4a**; without TBA, **Supplementary Fig. 2a** online) and E71T mutants (**Supplementary Fig. 2b**) were solved at 2.05- and 2.2-Å resolution, respectively. As expected, the distance between the carboxylate group of Asp80 and the hydroxyl group of Ser71 is 5.2 Å, too far to support any direct interaction. However, as predicted from molecular dynamics simulations, we found a crystallographic water connecting these residues through a well-defined set of hydrogen bonds, as shown in the $F_o - F_c$ omit map (**Fig. 4a**, inset). This relay water allows an interaction (albeit weaker) between the pore helix and external vestibule that would account for the mutant's intermediate inactivated phenotype (**Fig. 1c**). An interesting observation from the molecular dynamics simulation is the occupancy of this water molecule. In a 4-ns simulation, water is present in between Asp80 and E71S two-thirds of the time (data not shown), an amount that corresponds well with the strength of this interaction. Furthermore, the *B*-factor for this water in the crystal structure is 40 Å^2, about twice that of the well-ordered water (20 Å^2) behind the filter. These two findings suggest that the water molecule is disordered, and this could account for the intermediate phenotype of E71S.

The interaction between His71 and Asp80 seems to be strong enough to promote a deeply inactivated state (**Fig. 1c** and **Fig. 3a**). Thus, E71H represents a promising target for the structural determination of the inactivated state of the selectivity filter. Though we have vigorously pursued this, we have been unsuccessful in our attempts to determine the crystal structure of E71H mutant, mostly owing to its altered interaction with the Fab fragment required for a high-resolution structure (see **Supplementary Fig. 3** online). Taking an alternative approach, we used molecular dynamics simulations to characterize the effect of the E71H mutation on the transition to the C-type inactivated form of the filter. *In silico* mutation of WT KcsA to E71H$^+$ (+ denotes the imidazolium form of the side chain) and subsequent equilibration of the system (**Fig. 4b**) showed that the selectivity filter becomes unstable (r.m.s. deviation = 1.5 Å) shortly after constraints are released, affecting K$^+$-binding sites (**Supplementary Video 1** online).

Analysis of the 1-ns molecular dynamics trajectory of E71H led to three important conclusions. First, the presence of oppositely charged residues in a low dielectric cavity results in instantaneous formation of a salt bridge between His71 and Asp80 (**Fig. 4b**). Second, compared to the distance between Ala71 and Asp80 in the E71A simulation (**Supplementary Video 2** online), the Cα–Cα distance between His71 and Asp80 is 1–2 Å shorter (**Fig. 4c**) as a result of the strong interaction between these two residues. This in turn leads to considerable deformation of the selectivity filter and pinching at K$^+$-binding site 1 (S1; see **Fig. 4b**). Third, unlike equivalent simulations with WT and E71A channels, ions move from their initial S0-S2-S4 configuration to a new, S1-S4 arrangement, with the ion leaving the external binding site S0. A similar mechanism has been correlated to C-type inactivation in Shaker[24] (**Fig. 4b**, upper right). These results establish that the nature of the hydrogen bond network at the selectivity filter, including key interactions between positions 71 and

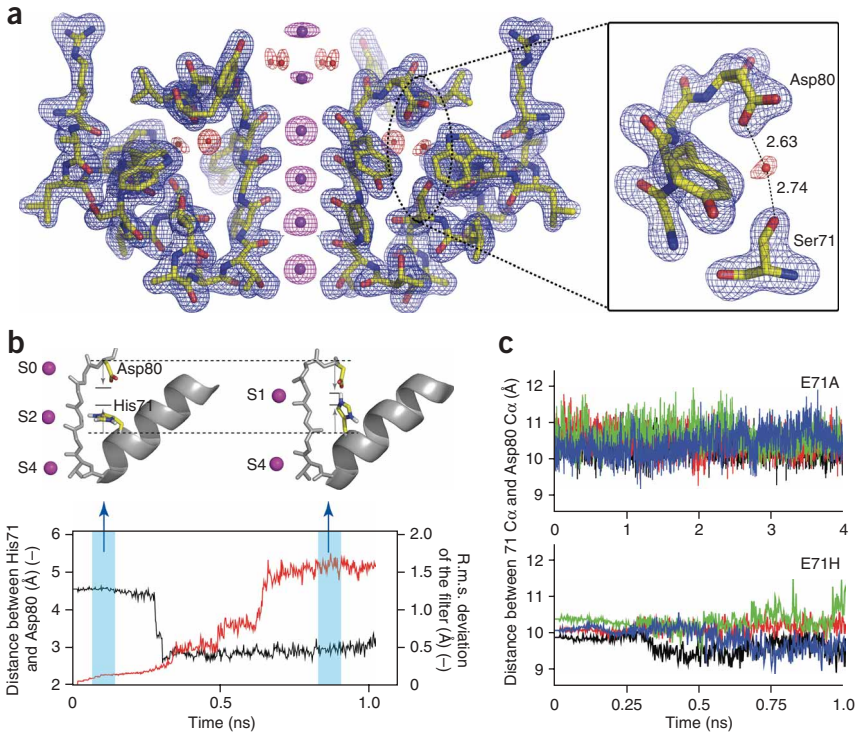

Figure 4 Structural basis of inactivation in E71S and E71H channels. (**a**) Crystal structure of E71S with TBA at 2.05-Å resolution. Shown is $F_o - F_c$ omit map of the filter corresponding to residues 64–82 from two diagonally symmetric subunits. The polypeptide chain is in stick representation and the blue mesh corresponds to the $F_o - F_c$ electron density map at $\sigma = 3.0$. Ions and water are represented as spheres, with $\sigma = 5.0$ for the ions (magenta mesh; two outermost ions are at $\sigma = 2.5$) and $\sigma = 3.0$ for the water molecules (red mesh). Inset, single-subunit representation of the hydrogen bond between E71S and Asp80 mediated through a crystallographic water. (**b**) Time series of the distance between E71H and Asp80 in our simulation, and r.m.s. deviation of the filter. After release of the constraints, the minimum distance between His71 and Asp80 is sharply reduced (black, left *y*-axis), and the filter is then distorted (red, right *y*-axis). Simulation was stopped at 1 ns, after filter became distorted. Initial configuration of the channel had the His71 rotamer pointed away from Asp80 (upper left structure). About 300 ps into the simulation (constraints released), an ion-pair interaction was formed between His71 and Asp80 (upper right structure). (**c**) Distance between position 71 Cα and Asp80 Cα, monitored for E71A and E71H. Each color represents a monomer.

80, determines both the stability of the conductive conformation and its entry into the nonconductive C-type inactivated state.

The driving forces of C-type inactivation

The present set of mutants afforded us the opportunity to probe the structural and energetic aspects of the selectivity filter interactions responsible for C-type inactivation in KcsA. Molecular dynamics simulations of the WT, E71A, E71S and E71H constructs were used to examine individual stabilities, the conformational dynamics of the selectivity filter and the effects of different side chain pairings to Asp80. What, then, determines the rate and extent of C-type inactivation in this group of mutants?

We first found a very strong correlation between nominal open probability and the strength of the interaction in the X71-Asp80 pair (**Fig. 5**), where X stands for any of the tested side chains. We defined interaction strength as the number of hydrogen bonds (plus an electrostatic component in the case of E71H) associated with residues Trp67, X71 and Asp80 in each case (**Fig. 5**, number in parentheses). Interaction strength, in turn, directly correlates with the X71-Asp80 Cα–Cα equilibrium distance in each mutant (indicated by crystallography and molecular dynamics simulations). For instance, the Cα–Cα distance in the two crystal structure forms of the non-inactivating E71A mutant ranges between 10 and 12.5 Å (ref. 17) and fluctuates near 11 Å in molecular dynamics simulations. In the molecular dynamics trajectories, the increasingly inactivating E71S, WT and E71H channels showed Cα–Cα distance distributions centered around 10.4, 9.9 and 9.6 Å, respectively (**Supplementary Fig. 4** online). On the basis of these results, we propose that the open conductive states of the E71S, WT and E71H channels, respectively, are increasingly unstable, as a consequence of the hydrogen bond network between positions in the pore helix (residue 71) and the external vestibule of the pore (residue 80). Interactions between these two sites promote compression of the selectivity filter parallel to the permeation pathway, which energetically biases it toward the inactivated conformation.

To test the stability and conformational dynamics of the selectivity filter, we probed the structural and energetic aspects of C-type inactivation in KcsA through additional molecular dynamics simulations. We calculated, using umbrella sampling simulations[27], the

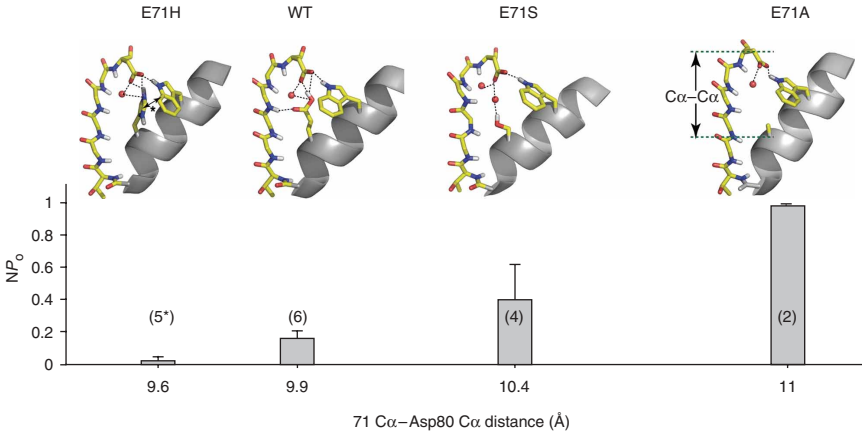

Figure 5 Relation between the open-channel probability (evaluated from Gaussian fits of histograms of all time points) and equilibrium X71-Asp80 Cα–Cα distance extracted from molecular dynamics simulations and crystal structures. Within parentheses is the number of hydrogen bond interactions involving residues 67, 71 and 80, for each variant. Asterisk denotes that the number includes extra cation-π (protonated E71H and Trp67) and ionic (protonated E71H and Asp80) interactions in E71H, apart from the hydrogen bond network. Data shown are means ± s.d. $n > 10$.

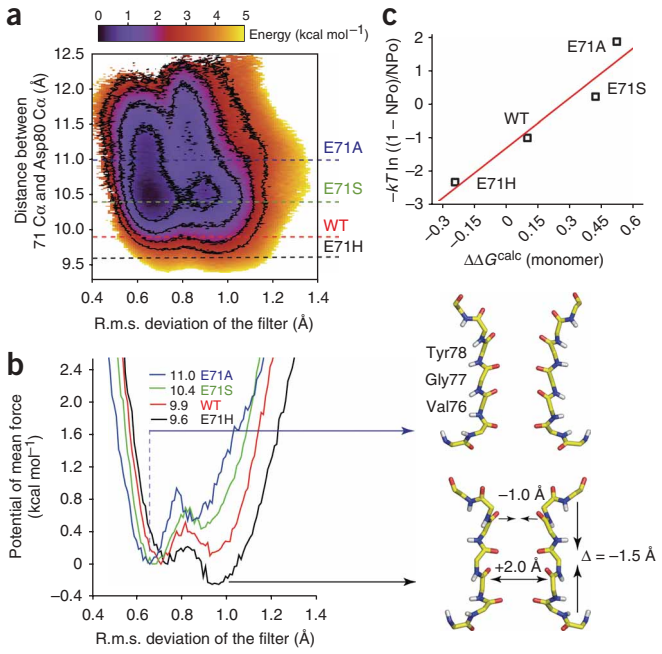

Figure 6 Correlation between the extent of inactivation and the energetics of filter distortion. (**a**) 2D-PMF with r.m.s. deviation of the filter and distance between X71 Cα and Asp80 Cα as the reaction coordinates. Each contour level corresponds to an energy of 0.75 kcal mol^{-1}. (**b**) 1D-PMF extracted from 2D-PMF using Boltzmann averaging of energy at Cα–Cα distances of 9.6 ± 0.25 (E71H-like), 9.9 ± 0.25 (WT-like), 10.4 ± 0.25 (E71S-like) and 11.0 ± 0.25 (E71A-like). Right, structures of the filter extracted from the simulation with r.m.s. deviation of 0.6 Å and X71-Asp80 Cα–Cα distance of 11.0 Å, similar to the putative conductive conformation (top), and with r.m.s. deviation of 1.1 Å and X71-Asp80 Cα–Cα distance of 9.6 Å, a putative nonconductive conformation (bottom). (**c**) Correlation of the calculated $\Delta\Delta G$ between putative conductive and inactivated filter structures for channels having four different side chain substitutions at position 71 with the experimentally determined ratio of conductive to nonconductive probabilities. The straight line corresponds to a linear fit ($y = 4.9x - 1.2$) with $R^2 = 0.92$.

free-energy surface or potential of mean force (PMF) corresponding to the filter conformation, as a function of the backbone distance (Cα–Cα) between positions 71 and 80. The free-energy landscape (**Fig. 6a**) is a two-dimensional PMF carried along two reaction coordinates, r.m.s. deviation of the filter and Cα–Cα distance. The 'L'-shaped surface clearly shows two minima, one at an r.m.s. deviation of 0.6 Å corresponding to a normal selectivity filter, favored at longer Cα–Cα distances, and a second one at an r.m.s. deviation of ~0.9 Å for smaller Cα–Cα distances, putatively associated with a nonconductive conformation of the selectivity filter. This is best revealed by sections of the PMF (**Fig. 6b**) extracted at average distances corresponding to the WT channel (9.9 Å) and the mutants showing effects on inactivation (E71A, 11 Å; E71S, 10.4 Å; E71H, 9.6 Å). When the PMF energies are normalized to the 0.6-Å r.m.s. deviation of the conducting filter minimum, the relative positions of the second minimum ($\Delta\Delta G$ values) correlate well with the stabilization of the inactivated state, according to the sequence E71A < E71S < WT < E71H (**Fig. 6b,c**). This suggests that constricting the selectivity filter (the distance from X71 Cα to Asp80 Cα) parallel to the permeation pathway increases the stability of a distorted filter (pinching at the S1 binding site and increasing the diameter at the S2 and S3 binding sites). These changes resemble previously reported nonconductive filter structures, in spite of the presence of a bound Fab fragment[18,28] (**Fig. 6b**, bottom right, and **Supplementary Fig. 5** online). Moreover, the differences in the backbone dihedral angles of the canonical and noncanonical structures (**Fig. 6b**, right) suggest that Gly77 has a key role in the distortion of the filter, as it can absorb the conformational change by displacing itself in the Ramachandran plot and allowing rearrangement of the Val76 and Tyr78 dihedral angles. Previous theoretical calculations have demonstrated that reorientation of these residues could be correlated to C-type inactivation[29].

This interpretation is strongly supported by the presence of a linear correlation between the $\Delta\Delta G$ (**Fig. 6c**) for the conductive, putatively inactivated conformation of the selectivity filter (calculated from **Fig. 6b**) and the log of the ratio between the probabilities of the open and nonconductive states of the channel (measured from single-channel recordings; shown in **Fig. 5**). This result further demonstrates that entry into the C-type inactivated state is energetically favorable and driven principally by the strength of the interaction between the pore helix and the external vestibule in KcsA.

Engineering hydrogen bond networks in Kv channels

The extent to which a system of hydrogen bond interactions serves as the basis for C-type inactivation in K^+ channels was tested in Kv1.2, a voltage-gated K^+ channel from rat brain that belongs to the Shaker K^+ channel family[30]. In the absence of its β subunit, Kv1.2 shows little or no C-type inactivation. Eukaryotic Kv channels have a conserved valine in the position equivalent to Glu71 in KcsA, which is unable to engage in a direct interaction with the Asp80 equivalent (Asp379), whereas glutamate in that position might interact with Asp379 (**Fig. 7**, inset). Normalized macroscopic currents showed that in Kv1.2 a V370E substitution accelerated and enhanced the inactivation process, an effect similar to, though not as complete as, the result of the equivalent mutation in KcsA (**Fig. 7** and **Supplementary Table 1** online). A substitution to serine (V370S) also promoted inactivation, but to a lesser extent than did the V370E substitution. No currents were observed for homotetramers of the V370H mutant, but co-expression of WT and V370H proteins produces functional channels with faster inactivation than that of WT Kv1.2 (data not shown), implying that a histidine residue at position 370 also promotes inactivation by a similar mechanism to that in KcsA. These results suggest that inactivation at the selectivity filter of Kv channels can also be regulated by the hydrogen bond network between the pore helix and residues in the external vestibule adjacent to the selectivity filter.

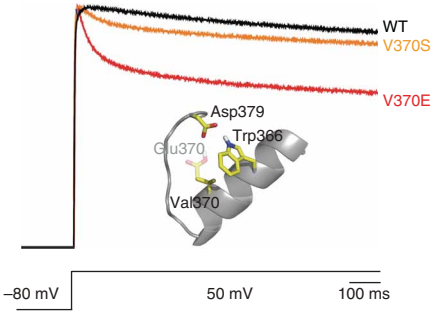

Figure 7 Mutations at position 370 recapitulate C-type inactivation in Kv1.2. (**a**) Normalized currents of mutants V370S and V370E elicited by a depolarizing voltage step from a holding potential of –80 mV to +50 mV. The inactivation rate of WT Kv1.2 speeds up considerably with the single amino acid substitution V370E or V370S. Inset shows a single subunit's P-loop with the interaction of Val370 (V370E transparent) and that of Asp379 in stick representation.

DISCUSSION

In response to prolonged stimulus, K^+ channels typically become nonconductive through a process known as slow, or C-type, inactivation. This has been associated with a distortion in the selectivity filter[4], and it is mechanistically distinct from N-type inactivation, which occurs intracellularly and involves a blocking particle within the permeation pathway[1]. C-type inactivation is crucial in establishing and controlling firing patterns in neurons[31] as well as in determining the length and frequency of the cardiac action potential[26,32]. The molecular events leading to loss of ion conduction at the selectivity filter have yet to be fully understood, but it is clear that a combination of functional information with static and dynamic structural information will be essential for this task. The present set of experiments provides a mechanistic explanation of the driving forces and suggests a molecular mechanism for the transition between the conductive and nonconductive states of the selectivity filter in K^+ channels.

There is compelling evidence suggesting that the selectivity filter has an important function in gating, acting as a second gate in a variety of K^+ channels[17,29,33–36]. Early data on the effects of permeant ions on gating[8,37,38] suggested that the selectivity filter might be involved in both the permeation and gating functions. Ions with longer occupancy in the selectivity filter (Rb^+, Cs^+ and NH_4^+) tend to slow down entry into the inactivated state through a 'foot-in-the-door' mechanism in which the resident ion stabilizes the conductive conformation[8,37]. Furthermore, the occurrence of subconductance current levels with altered selectivity is associated with mutations in the selectivity filter[39,40]. Mutations in the selectivity filter[14] or surrounding structure[11,15,33,41] have large effects on rapid gating transitions, whereas other mutations strongly influence the kinetics and extent of C-type inactivation. Moreover, an increase in K^+ concentration or binding of the blocker TEA in the extracellular region considerably decreases C-type inactivation[6,7,24]. These results suggest that the selectivity filter and its associated support structures (the pore helix and turret loop) are key in the gating process, both at slow (C-type inactivation) and fast (single-channel flicker) timescales.

Several lines of evidence point to a mechanistic equivalence between KcsA inactivation and C-type inactivation in eukaryotic voltage-dependent K^+ channels. Mutation of Tyr82 (functionally equivalent to Thr449 in Shaker and Ser631 in HERG), and mutation of Glu71 (functionally equivalent to Val438 in Shaker and Ser620 in HERG) affect the rate and extent of inactivation[7,12,13]. Additionally, the rate of C-type inactivation in KcsA depends on extracellular K^+ to a similar extent as does inactivation in its eukaryotic counterparts[17]. Given the high degree of sequence conservation in the K^+ channel selectivity filter, we expect that these channels have a common mechanism of C-type inactivation.

We have shown that conformational changes at the selectivity filter of KcsA exert an important effect in the inactivation gating process, particularly those involving interactions between residues Trp67 and Glu71 at the pore helix and Asp80 at the end of the signature sequence in the mouth of the pore[17]. Disrupting the interaction between residues Glu71 and Asp80 relieves C-type inactivation in KcsA, and the mutation E71A essentially abolishes it, boosting the steady-state open probability. Using CW-EPR spectroscopic measurements and fluorescence lifetime spectroscopy in combination with pore mutants with very different open probabilities[17,36], we have previously shown that once the intracellular gate formed by the TM2 helices is maximally activated, it has a minimal role in stationary gating. On the basis of these results, we proposed a model in which the selectivity filter is intrinsically unstable and movement of the TM2 gate allows the selectivity filter to undergo a rearrangement that leads to a more stable inactivated state.

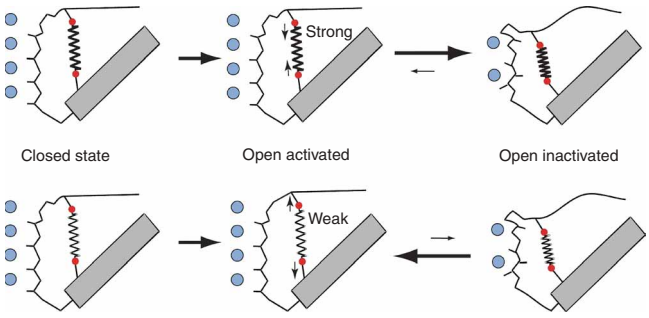

Figure 8 Structural rearrangement during C-type inactivation at the filter. Shown is a cartoon representation of molecular events during KcsA gating (see text for details).

Previous work[4] has suggested that C-type inactivation involves a local rearrangement and constriction of the outer mouth of the Shaker K^+ channel. Our results agree with this finding, as shown by pinching of the S1 site in KcsA in molecular dynamics simulations. However, we propose that this conformational change in the outer mouth is a consequence of a preceding event driven by the network of interactions between the pore helix and the external vestibule, as indicated by electrophysiological measurements and molecular dynamics simulations. This set of interactions promotes constriction of the selectivity filter parallel to the permeation pathway, leading to distortion of the filter (**Fig. 6b**). This configuration is reminiscent of previously determined structures of WT KcsA at a low K^+ concentration[18] and in the presence of intracellular blockers[28] (**Supplementary Fig. 5**), and of the M96V mutant[42]. It is tempting to link these collapsed filter structures to an inactivated state, though it should be considered that these crystal structures and our present computational model (biased to a closed-inactivated conformation) were obtained with the channel's inner gate (TM2) in its closed conformation. Nevertheless, the closed-inactivated state observed at the functional level in Shaker channels[24,25,43] supports the idea that the reported structures form the basis for an inactivated state even when the lower gate is closed. We consider it plausible that the closed-inactivated structure (see above) might be maintained in the open state. However, determining the final structural correlate of the C-type inactivated state will probably require solving the structure of an open-inactivated channel. Given the stability of the inactivated conformation of the filter induced by the His71-Asp80 interaction in the E71H channel, this mutant remains a viable candidate for the structure of a closed-inactivated form of the filter.

A mechanistic interpretation of our results is summarized in **Figure 8**. The stability of the selectivity filter is modulated by a series of interactions pictured as 'molecular springs'. Weakening one of the key springs in the network (E71A mutant, bottom diagrams) stabilizes the conductive state of the filter. Increasing the strength of the spring (E71H mutation, top diagrams) stabilizes the nonconductive state by causing a decrease in the distance between X71 Cα and Asp80 Cα, which induces pinching at the S1 site and promotes widening of the S2 and S3 binding sites. Indeed, we find that the differences in the rate of inactivation between WT KcsA and mutants result from the strengths of interactions involving residues in the pore helix and external vestibule, according to the sequence E71A < E71S < WT < E71H (**Fig. 5**). We suggest that the overall mechanism diagrammed in **Figure 8** might represent the actual events that occur during the transition from the conductive to nonconductive state of the WT KcsA selectivity filter.

However, in comparison to KcsA, Kv channels present an apparently more complex mechanism. Even though the Glu71-Asp80 molecular spring corresponding to KcsA is absent, other interactions might have equivalent roles during the C-type inactivation process (**Supplementary Fig. 6** online). Nevertheless, as shown above, C-type inactivation in Kv channels can be enhanced by the addition of a KcsA-equivalent molecular spring. Together, the present results in KcsA and Kv1.2 provide a framework for understanding the molecular mechanism of C-type inactivation in K^+ channels.

METHODS

Mutagenesis and channel biochemistry. We used a pQE32 vector encoding KcsA for protein expression, as described[17,19,22,44]. For E71H purification (**Supplementary Fig. 3a**), we changed the conventional expression and purification protocol in several ways to preserve the oligomeric properties of this mutant. Induction was carried out with 0.5 mM IPTG in the presence of 10% (v/v) glycerol and 10 mM Ba^{2+} at 27 °C for 6 h. Membranes containing the E71H channel were solubilized for 3 h at 4 °C in 200 mM KCl, 50 mM Tris, 10% (v/v) glycerol and 10 mM *n*-dodecyl-β-D-maltopyranoside (DDM) (pH 8), and then incubated for 3 h at 4 °C with Co^{2+}-based metal-chelate chromatography resin. For EPR measurements, purified mutants were spin-labeled with methanethiosulfonate spin label (Toronto Research) at a 10:1 label/channel molar ratio and reconstituted in asolectin vesicle by dilution in PBS (pH 8) followed by additional detergent extraction with biobeads[45].

Liposome patch clamp. We made electrophysiological measurements of proteoliposomes using the patch-clamp method described[46]. Single-channel recordings were obtained from a 1:5,000–10,000 (mass/mass) ratio of protein to lipid. Macroscopic currents were measured at a 1:100 ratio, except for the E71H mutant, for which the ratio was 1:25. Except where another method is explicitly described, we made patch-clamp measurements under symmetrical conditions, in 200 mM KCl and 5 mM MOPS buffer (pH 4.0). We recorded single-channel currents with an Axopatch 200B device and sampled currents at 40 kHz with the analog filter set to 5 kHz (–3 dB). Pipette resistances were 1.7–2 MΩ. We recorded macroscopic currents after a pH jump using an RCS-160 fast-solution exchanger (Biologic). Single-channel analyses were done using pCLAMP 9 (Axon Instruments). We idealized the currents through the half-amplitude threshold algorithm at 2 kHz.

Two-electrode voltage clamp. We prepared complementary RNA from rat Kv1.2 (rKv1.2, GenBank X16003) with the mMESSAGE mMACHINE T7 kit (Ambion) after linearization of plasmid complementary DNA. Defolliculated stage IV and V *Xenopus laevis* oocytes were injected with 5 ng WT or mutant rKv1.2 complementary RNA and cultured in ND96 supplemented with 50 μg ml^{-1} gentamycin and 1% (v/v) penicillin-streptomycin at 16 °C. We measured whole-cell currents 48 h after injection using a Geneclamp 500 amplifier (Axon Instruments). Data were sampled at 5 kHz and recorded using Clampex software (Axon Instruments). Leak and capacitance was subtracted online using standard pulse-subtraction protocols. The bath solution was 96 mM NaCl, 4 mM KCl, 1 mM $MgCl_2$, 0.3 mM $CaCl_2$ and 10 mM HEPES (pH 7.6).

Electron paramagnetic resonance spectroscopy. We obtained X-band CW-EPR spectra from spin-labeled and reconstituted channels as described[22], using a Bruker ELEXYS spectrometer equipped with a loop-gap resonator under the following conditions: 2 mW incident power, 100 kHz modulation frequency and 1 G modulation amplitude. All spectra were obtained at room temperature.

X-ray crystallography. We crystallized KcsA (pQE32 vector) mutant E71S in the presence or absence of 5 mM TBA, as well as KcsA mutant E71T, in the presence of an Fab antibody fragment, as described[18]. Beam-like crystals of KcsA–Fab complex appeared after 1 week in a sitting drop containing 23%–26% (v/v) PEG 400, 50 mM magnesium acetate and 50 mM sodium acetate (pH 4.8–5.4) at 19 °C. Crystals diffracted to a Bragg spacing of 2.05 Å for E71S with TBA, 2.2 Å for E71T, and 2.3 Å for E71S without TBA. Data were collected at the GM/CA-23-ID beamline at the Advanced Photon Source and processed with HKL2000 (ref. 47). E71 mutant structures were solved by molecular replacement using the WT KcsA–Fab complex structure (PDB 1K4C) as search model. All the structures were solved using Fab and KcsA without the selectivity filter as the initial model for molecular replacement. Refinement of the structures was carried out through multiple cycles of manual rebuilding using O[48] and refinement using CNS[49]. Data collection and refinement statistics are given in **Table 1**.

Table 1 Data collection and refinement statistics

	KcsA E71S with TBA
Data collection	
Space group	*I*4
Cell dimensions	
a, *b*, *c* (Å)	156.34, 156.34, 76.0
Resolution (Å)	50.0–2.05
R_{merge} (%)	5.0 (26.9)
$I / \sigma I$	33.5 (4.5)
Completeness (%)	99.5 (97.8)
Redundancy	4.4 (4.1)
Refinement	
Resolution (Å)	50.0–2.05
No. reflections	50,887
R_{work} / R_{free} (%)[a]	21.9 / 23.4
No. atoms	
Protein	4,071
Ion	6
Lipid	41
Water	155
B-factors	
Protein	55.94
Ion	35.70
Water	50.33
R.m.s. deviations	
Bond lengths (Å)	0.006
Bond angles (°)	1.285

Values in parentheses are for the highest-resolution shell (2.15–2.05 Å).
[a]10% of the data, which were excluded in the refinement, were used in the R_{free} calculation.

Molecular dynamics. The simulation system was represented by an atomic model of the KcsA channel (PDB 1K4C) embedded in dipalmitoylphosphatidylcholine (DPPC) surrounded by an aqueous solution of 150 mM KCl. The microscopic system was composed of a KcsA tetramer of 404 amino acid residues (6,284 atoms), 112 DPPC molecules, 6,384 water molecules and 3 K^+ ions in the pore (S0, S2 and S4 positions in the selectivity filter). To make the entire system electrically neutral, we added 6 K^+ and 21 Cl^- ions in the bulk solution to mimic 150 mM KCl. We performed all the calculations using c29a2 or c32a2 of the biomolecular simulation program CHARMM[50]. The simulation methodology has been described[51]. Different E71 mutants were generated *in silico* and carefully equilibrated before the production run. For the umbrella sampling PMF calculations, we generated a total of 180 independent E71A simulations of 2 ns, using a biasing harmonic potential centered on the r.m.s. deviation of the filter (varying successively from 0 to 2 every 0.1 Å) and the X71-Asp80 Cα–Cα distance (varying successively from 8.5 to 12.5 every 0.5 Å), with force constants of 40 kcal mol^{-1} $Å^{-2}$ and 10 kcal mol^{-1} $Å^{-2}$, respectively. We unbiased all the biased simulations using the weighted histogram analysis method (WHAM)[52] to calculate the full PMF. First, we performed molecular dynamics simulations in the presence of an artificial biasing potential on the r.m.s. deviation of the selectivity filter to obtain the entire conformational space traversed by the filter at a given Cα–Cα distance. Next, we removed the bias introduced by this potential to obtain the unbiased free-energy surface of the system.

Accession codes. Protein Data Bank: Coordinates have been deposited with accession code 2P7T.

Note: Supplementary information is available on the Nature Structural & Molecular Biology website.

ACKNOWLEDGMENTS

We thank F. Bezanilla, S. Chakrapani, L. Cuello, M. Sotomayor and H. Raghuraman for critical reading and discussion of the manuscript; M. Wiener and M. Purdy for crystallographic data collection (for E71T); J. Faraldo-Gomez and A. Lau for critical comments on the PMF calculations; S. Goldstein (University of Chicago) for providing access to the two electrode voltage clamp system; the staff of the GM/CA-23-ID beamline at the Advanced Photon Source for their invaluable assistance in data collection; R. MacKinnon (Rockefeller University) for providing the KcsA antibody hybridoma cell line; and the National Center for Supercomputing Applications and Jazz computing cluster at Argonne National Laboratory for computer time. This work was supported by US National Institutes of Health grants to E.P. and B.R.

AUTHOR CONTRIBUTIONS

J.F.C.-M. carried out the channel mutagenesis, biochemistry, EPR studies, crystallization and electrophysiology with KcsA channels, and J.F.C.-M. and A.L. carried these out on Kv1.2 channels. V.J. carried out crystal data collection, structure solving and computational analyses. V.V. participated in channel mutagenesis, biochemistry and EPR. D.M.C. made all the Fab preparations. B.R., working with V.J., participated in computational design and PMF calculations. E.P. directed experimental design and data analyses, and wrote the manuscript with J.F.C.-M., V.J. and B.R.

Published online at http://www.nature.com/nsmb/
Reprints and permissions information is available online at http://npg.nature.com/reprintsandpermissions

1. Hoshi, T., Zagotta, W.N. & Aldrich, R.W. Two types of inactivation in Shaker K^+ channels: effects of alterations in the carboxy-terminal region. *Neuron* **7**, 547–556 (1991).
2. Yellen, G. The moving parts of voltage-gated ion channels. *Q. Rev. Biophys.* **31**, 239–295 (1998).
3. Yellen, G., Sodickson, D., Chen, T.Y. & Jurman, M.E. An engineered cysteine in the external mouth of a K^+ channel allows inactivation to be modulated by metal binding. *Biophys. J.* **66**, 1068–1075 (1994).
4. Liu, Y., Jurman, M.E. & Yellen, G. Dynamic rearrangement of the outer mouth of a K^+ channel during gating. *Neuron* **16**, 859–867 (1996).
5. Kiss, L., LoTurco, J. & Korn, S.J. Contribution of the selectivity filter to inactivation in potassium channels. *Biophys. J.* **76**, 253–263 (1999).
6. Choi, K.L., Aldrich, R.W. & Yellen, G. Tetraethylammonium blockade distinguishes two inactivation mechanisms in voltage-activated K^+ channels. *Proc. Natl. Acad. Sci. USA* **88**, 5092–5095 (1991).
7. Lopez-Barneo, J., Hoshi, T., Heinemann, S.H. & Aldrich, R.W. Effects of external cations and mutations in the pore region on C-type inactivation of Shaker potassium channels. *Receptors Channels* **1**, 61–71 (1993).
8. Demo, S.D. & Yellen, G. Ion effects on gating of the Ca^{2+}-activated K^+ channel correlate with occupancy of the pore. *Biophys. J.* **61**, 639–648 (1992).
9. Kurata, H.T. & Fedida, D. A structural interpretation of voltage-gated potassium channel inactivation. *Prog. Biophys. Mol. Biol.* **92**, 185–208 (2006).
10. Seebohm, G., Sanguinetti, M.C. & Pusch, M. Tight coupling of rubidium conductance and inactivation in human KCNQ1 potassium channels. *J. Physiol. (Lond.)* **552**, 369–378 (2003).
11. Chapman, M.L., Blanke, M.L., Krovetz, H.S. & Vandongen, A.M. Allosteric effects of external K^+ ions mediated by the aspartate of the GYGD signature sequence in the Kv2.1 K^+ channel. *Pflugers Arch.* **451**, 776–792 (2006).
12. Ficker, E., Jarolimek, W., Kiehn, J., Baumann, A. & Brown, A.M. Molecular determinants of dofetilide block of HERG K^+ channels. *Circ. Res.* **82**, 386–395 (1998).
13. Yifrach, O. & MacKinnon, R. Energetics of pore opening in a voltage-gated K^+ channel. *Cell* **111**, 231–239 (2002).
14. Lu, T. *et al.* Probing ion permeation and gating in a K^+ channel with backbone mutations in the selectivity filter. *Nat. Neurosci.* **4**, 239–246 (2001).
15. Alagem, N., Yesylevskyy, S. & Reuveny, E. The pore helix is involved in stabilizing the open state of inwardly rectifying K^+ channels. *Biophys. J.* **85**, 300–312 (2003).
16. Gao, L., Mi, X., Paajanen, V., Wang, K. & Fan, Z. Activation-coupled inactivation in the bacterial potassium channel KcsA. *Proc. Natl. Acad. Sci. USA* **102**, 17630–17635 (2005).
17. Cordero-Morales, J.F. *et al.* Molecular determinants of gating at the potassium-channel selectivity filter. *Nat. Struct. Mol. Biol.* **13**, 311–318 (2006).
18. Zhou, Y., Morais-Cabral, J.H., Kaufman, A. & MacKinnon, R. Chemistry of ion coordination and hydration revealed by a K^+ channel-Fab complex at 2.0 Å resolution. *Nature* **414**, 43–48 (2001).
19. Cordero-Morales, J.F., Cuello, L.G. & Perozo, E. Voltage-dependent gating at the KcsA selectivity filter. *Nat. Struct. Mol. Biol.* **13**, 319–322 (2006).
20. Kuo, A. *et al.* Crystal structure of the potassium channel KirBac1.1 in the closed state. *Science* **300**, 1922–1926 (2003).
21. Yang, J., Yu, M., Jan, Y.N. & Jan, L.Y. Stabilization of ion selectivity filter by pore loop ion pairs in an inwardly rectifying potassium channel. *Proc. Natl. Acad. Sci. USA* **94**, 1568–1572 (1997).
22. Perozo, E., Cortes, D.M. & Cuello, L.G. Three-dimensional architecture and gating mechanism of a K^+ channel studied by EPR spectroscopy. *Nat. Struct. Biol.* **5**, 459–469 (1998).
23. Perozo, E., Cortes, D.M. & Cuello, L.G. Structural rearrangements underlying K^+-channel activation gating. *Science* **285**, 73–78 (1999).
24. Baukrowitz, T. & Yellen, G. Modulation of K^+ current by frequency and external $[K^+]$: a tale of two inactivation mechanisms. *Neuron* **15**, 951–960 (1995).
25. Panyi, G. & Deutsch, C. Cross talk between activation and slow inactivation gates of Shaker potassium channels. *J. Gen. Physiol.* **128**, 547–559 (2006).
26. Smith, P.L., Baukrowitz, T. & Yellen, G. The inward rectification mechanism of the HERG cardiac potassium channel. *Nature* **379**, 833–836 (1996).
27. Torrie, G.M. & Valleau, J.P. Nonphysical sampling distributions in Monte Carlo free-energy estimation: umbrella sampling. *J. Comp. Phys.* **23**, 187–199 (1977).
28. Lenaeus, M.J., Vamvouka, M., Focia, P.J. & Gross, A. Structural basis of TEA blockade in a model potassium channel. *Nat. Struct. Mol. Biol.* **12**, 454–459 (2005).
29. Berneche, S. & Roux, B. A gate in the selectivity filter of potassium channels. *Structure* **13**, 591–600 (2005).
30. Stuhmer, W. *et al.* Molecular basis of functional diversity of voltage-gated potassium channels in mammalian brain. *EMBO J.* **8**, 3235–3244 (1989).
31. Bean, B.P. The action potential in mammalian central neurons. *Nat. Rev. Neurosci.* **8**, 451–465 (2007).
32. Spector, P.S., Curran, M.E., Zou, A., Keating, M.T. & Sanguinetti, M.C. Fast inactivation causes rectification of the IKr channel. *J. Gen. Physiol.* **107**, 611–619 (1996).
33. Sun, Z.P., Akabas, M.H., Goulding, E.H., Karlin, A. & Siegelbaum, S.A. Exposure of residues in the cyclic nucleotide-gated channel pore: P region structure and function in gating. *Neuron* **16**, 141–149 (1996).
34. Bruening-Wright, A., Schumacher, M.A., Adelman, J.P. & Maylie, J. Localization of the activation gate for small conductance Ca^{2+}-activated K^+ channels. *J. Neurosci.* **22**, 6499–6506 (2002).
35. Claydon, T.W., Makary, S.Y., Dibb, K.M. & Boyett, M.R. The selectivity filter may act as the agonist-activated gate in the G protein-activated Kir3.1/Kir3.4 K^+ channel. *J. Biol. Chem.* **278**, 50654–50663 (2003).
36. Blunck, R., Cordero-Morales, J.F., Cuello, L.G., Perozo, E. & Bezanilla, F. Detection of the opening of the bundle crossing in KcsA with fluorescence lifetime spectroscopy reveals the existence of two gates for ion conduction. *J. Gen. Physiol.* **128**, 569–581 (2006).
37. Swenson, R.P., Jr & Armstrong, C.M. K^+ channels close more slowly in the presence of external K^+ and Rb^+. *Nature* **291**, 427–429 (1981).
38. Spruce, A.E., Standen, N.B. & Stanfield, P.R. Rubidium ions and the gating of delayed rectifier potassium channels of frog skeletal muscle. *J. Physiol. (Lond.)* **411**, 597–610 (1989).
39. Chapman, M.L., VanDongen, H.M. & VanDongen, A.M. Activation-dependent subconductance levels in the drk1 K channel suggest a subunit basis for ion permeation and gating. *Biophys. J.* **72**, 708–719 (1997).
40. Zheng, J. & Sigworth, F.J. Intermediate conductances during deactivation of heteromultimeric Shaker potassium channels. *J. Gen. Physiol.* **112**, 457–474 (1998).
41. Proks, P., Capener, C.E., Jones, P. & Ashcroft, F.M. Mutations within the P-loop of Kir6.2 modulate the intraburst kinetics of the ATP-sensitive potassium channel. *J. Gen. Physiol.* **118**, 341–353 (2001).
42. Lockless, S.W., Zhou, M. & MacKinnon, R. Structural and thermodynamic properties of selective ion binding in a K^+ channel. *PLoS Biol.* **5**, e121 (2007).
43. Claydon, T.W. *et al.* A direct demonstration of closed-state inactivation of K^+ channels at low pH. *J. Gen. Physiol.* **129**, 437–455 (2007).
44. Cortes, D.M. & Perozo, E. Structural dynamics of the *Streptomyces lividans* K^+ channel (SKC1): oligomeric stoichiometry and stability. *Biochemistry* **36**, 10343–10352 (1997).
45. Cuello, L.G., Romero, J.G., Cortes, D.M. & Perozo, E. pH-dependent gating in the *Streptomyces lividans* K^+ channel. *Biochemistry* **37**, 3229–3236 (1998).
46. Cortes, D.M., Cuello, L.G. & Perozo, E. Molecular architecture of full-length KcsA: role of cytoplasmic domains in ion permeation and activation gating. *J. Gen. Physiol.* **117**, 165–180 (2001).
47. Otwinowski, Z. & Minor, W. Macromolecular crystallography, part A. *Methods Enzymol.* **276**, 307–326 (1997).
48. Jones, T.A., Zou, J.-Y., Cowan, S.W. & Kjeldgaard, M. Improved methods for building protein models in electron density maps and the location of errors in these models. *Acta Crystallogr. A* **47**, 110–119 (1991).
49. Brunger, A.T. *et al.* Crystallography and NMR system: a new software suite for macromolecular structure determination. *Acta Crystallogr. D Biol. Crystallogr.* **54**, 905–921 (1998).
50. Brooks, B.R. *et al.* CHARMM: a program for macromolecular energy, minimization, and dynamics calculations. *J. Comput. Chem.* **4**, 187–217 (1983).
51. Berneche, S. & Roux, B. Molecular dynamics of the KcsA K^+ channel in a bilayer membrane. *Biophys. J.* **78**, 2900–2917 (2000).
52. Kumar, S., Bouzida, D., Swendsen, R.H., Kollman, P.A. & Rosenberg, J.M. The weighted histogram analysis method for free-energy calculations on biomolecules. I. The methods. *J. Comput. Chem.* **13**, 1011–1021 (1992).